Uncertainty propagation of phase contrast-MRI derived inlet boundary conditions in computational hemodynamics models of thoracic aorta

Silvia Bozzi[a], Umberto Morbiducci[b], Diego Gallo[b], Raffaele Ponzini[c], Giovanna Rizzo[d], Cristina Bignardi[b] and Giuseppe Passoni[a]

[a]Department of Electronics, Information Science, and Bioengineering, Politecnico di Milano, Milan, Italy; [b]Department of Mechanical and Aerospace Engineering, Politecnico di Torino, Turin, Italy; [c]HPC and Innovation Unit, CINECA, Milan, Italy; [d]IBFM, Research National Council, Milan, Italy

ABSTRACT

This study investigates the impact that uncertainty in phase contrast-MRI derived inlet boundary conditions has on patient-specific computational hemodynamics models of the healthy human thoracic aorta. By means of Monte Carlo simulations, we provide advice on where, when and how, it is important to account for this source of uncertainty. The study shows that the uncertainty propagates not only to the intravascular flow, but also to the shear stress distribution at the vessel wall. More specifically, the results show an increase in the uncertainty of the predicted output variables, with respect to the input uncertainty, more marked for blood pressure and wall shear stress. The methodological approach proposed here can be easily extended to study uncertainty propagation in both healthy and pathological computational hemodynamic models.

KEYWORDS

Phase contrast MRI; computational hemodynamics; thoracic aorta; wall shear stress; uncertainty propagation; boundary conditions

1. Introduction

In the last decades, computational fluid dynamics (CFD) has been extensively used to study cardiovascular flows, proving to be an effective tool to gain insights into the complex relationships between hemodynamics and pathophysiology. More recently, the coupling of computational hemodynamics and cardiovascular imaging has allowed to build up even more realistic and personalized CFD models in term of both anatomy and boundary conditions (Taylor & Steinman 2010). In particular, phase-contrast magnetic resonance imaging (PC-MRI) has been increasingly used to provide patient-specific vessel geometries and flow data, useful for setting fully personalized conditions at boundaries.

In general, the computation of hemodynamic quantities, enabled by the combination of *in vivo* imaging and CFD, requires some assumptions. As a result, the reliability of patient-specific CFD results strongly depends on the level of uncertainty introduced in the modelling process. Many sources of uncertainty can affect the accuracy of image-based CFD results: image acquisition and processing, mathematical modelling assumptions, physical parameter values and boundary condition (BC) settings. In particular, the latter are known to be relevant in the simulation of hemodynamic scenarios (Veneziani & Vergara 2005; Grinberg & Karniadakis 2008; Spilker & Taylor 2010; Gallo et al. 2012; D'Elia & Veneziani 2013; Morbiducci et al. 2013; Quarteroni et al. 2016).

To successfully translate CFD predictions into clinics, all the relevant uncertainty sources should be identified and propagated through the model equations to assess the level of uncertainty of the output variables of interest. This would allow to provide clinicians with model predictions together with the associated uncertainties, thus improving the added value of CFD tools in clinical practice.

Different numerical approaches have been used to quantify uncertainty propagation in blood flow simulations, starting from sampling techniques like Monte Carlo method (Huberts et al. 2012; Tran et al. 2017) to more compact projection-based methods as the polynomial chaos expansions (Sankaran & Marsden 2011; Quicken et al. 2016; Eck et al. 2017). A comparison between the two approaches has been presented by Eck et al. (2016), who showed that polynomial chaos expansions perform better for low dimensional problems, while Monte Carlo method is more suitable for higher dimension problems.

A number of studies have investigated the following sources of uncertainty in computational hemodynamics

CONTACT Silvia Bozzi silvia.bozzi@polimi.it

Received 6 December 2016
Accepted 22 May 2017

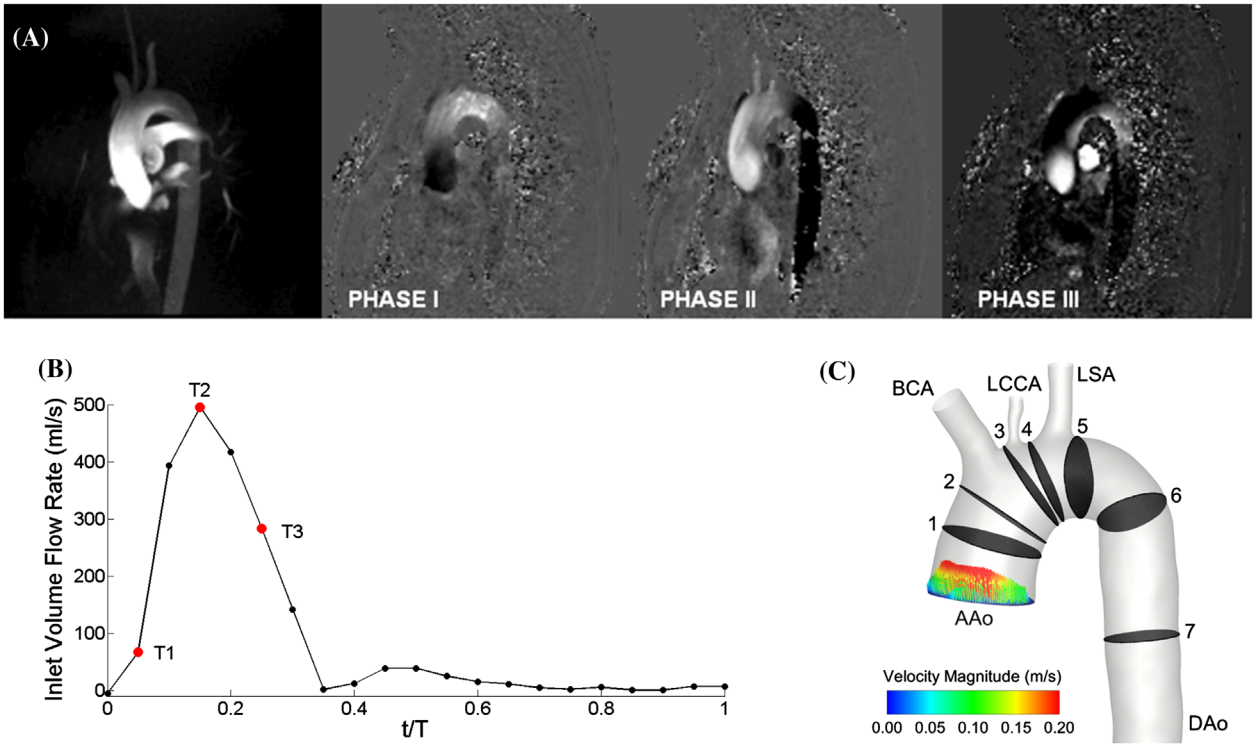

Figure 1. Panel A: 3D PC-MRI images of the thoracic aorta acquired at mid systole on a plane aligned with the aortic arch. From left to right, maximum intensity projection image, and the three-directional instantaneous phase velocity map frames (phase I, II, III), corresponding to the three components of the velocity vector field. Image brightness is proportional to signal intensity (a more contrasted gray scale was used for phase III, in order to better appreciate phase velocity distribution also for the smallest measured phase velocity). Panel B: Measured volume flow rate waveform at the ascending aorta. Time instants T1, T2 and T3 are selected for steady-state simulations. Panel C: Aortic geometry, as reconstructed from PC-MRI images. The time-averaged (along the cardiac cycle) three-dimensional velocity profile at the AAo inlet section is presented. Planes 1:7 used for post-processing are also shown. AAo: ascending aorta, BCA: brachiocephalic artery, LCCA: left common carotid artery, LSA: left subclavian artery, DAo: descending aorta.

models: reconstructed vessel geometry (Sankaran & Marsden 2011; Sankaran et al. 2015, 2016), input and output BCs (Sankaran & Marsden 2011; Morbiducci et al. 2013; Tiago et al. 2014; Valen-Sendstad et al. 2015; Schiavazzi et al. 2016; Tran et al. 2017), vessel distensibility and motion (Jin et al. 2003; Zhao et al. 2000; Eck et al. 2016; Javadzadegan et al. 2016) and rheological properties of blood (Lee & Steinman 2007; Morbiducci et al. 2011b). In a recent study, the Authors reported a numerical experiment in which different possible strategies of applying PC-MRI measured flow data as BCs in computational hemodynamic models of healthy human aorta were implemented (Morbiducci et al. 2013). The reported findings highlighted that the assumption of idealized velocity profiles as inlet BCs in personalized computational models can lead to misleading representations of aortic hemodynamics.

In this study, we make a further step in investigating the effect of one of the causes of uncertainty in image-based cardiovascular simulations, the PC-MRI derived Dirichlet condition, when applied at the inflow boundary. More in detail, the study shows how uncertainty affecting PC-MRI measurements of blood velocity profiles, applied as inflow BCs to a personalized model of healthy human aorta propagates from the inlet section at the ascending aorta through the region of interest and results in specific uncertainty of blood flow predictions. By means of a set of Monte Carlo simulations, we attempt to provide advice on where, when and how, in personalized computational hemodynamic models of the human aorta, it is important to account for inlet BCs uncertainty affecting velocity profiles. The results are analyzed in terms of some blood flow descriptors at different locations along the ascending aorta and the aortic arch. The final goal is to obtain accurate and reliable information useful to diagnostic/prognostic purposes.

2. Methods

2.1. PC-MRI data

4D PC-MRI images were used to obtain the anatomic model of a healthy human thoracic aorta (Figure 1). The healthy volunteer object of the study is male, age 42 years, weight 60 kg. The subject is part of the data-set analyzed in Morbiducci et al. (2011a).

The MRI data sequence was extensively detailed in several previous studies (Morbiducci et al. 2009; Morbiducci et al. 2011a; Tresoldi et al. 2014; Volonghi et al. 2016), and reported in other computational hemodynamics studies (Gallo et al. 2012; Morbiducci et al. 2013, 2015). Briefly, 4D MRI images of an ostensibly healthy human aorta were acquired using a 1.5 T scanner (Achieva, Philips Healthcare, The Netherlands). Blood phase velocity and anatomical data were acquired in 22 oblique sagittal slices (field of view 280 × 280 mm^2) aligned with the aortic arch and the entire aorta was covered with an isotropic spatial sampling (voxel size equal to 2 × 2 mm^2; slice thickness 4 mm, 2 mm slice spacing). A gradient echo spin sequence was used with velocity encoding (VENC) in all three directions (scan parameters: TR/TE = 5.4/3 ms; VENC = 150 cm s^{-1}). Motion artifacts were minimized using a navigator echo approach. The PC pulse sequence was arranged to allow synchronization of the data to the cardiac cycle. This allowed to reconstruct a cine series of 3D data sets from multiple phases of the cardiac cycle. The resulting cine pulse sequence was retrospectively gated to the electrocardiographic cycle to obtain 22 cardiac phases.

The geometry (Figure 1) is characterized by an inlet section at the ascending aorta (AAo) and multiple outlets at the descending aorta (DAo) and at the supra-aortic vessels: brachiocephalic artery (BCA), left common carotid artery (LCCA) and left subclavian artery (LSA). The surface area of the inlet section is equal to $9.61 \cdot 10^{-4}$ m^2. As for the outflow boundaries, the surface areas of the outlet sections of the model are: DAo = $3.66 \cdot 10^{-4}$ m^2, BCA = $9.18 \cdot 10^{-5}$ m^2, LCCA = $1.63 \cdot 10^{-5}$ m^2, LSA = $5.30 \cdot 10^{-5}$ m^2. To investigate uncertainty propagation, seven cross-sections – perpendicular to local vessel's axis - were selected along the thoracic aorta, at relevant anatomical landmarks (Figure 1).

PC-MRI phase flow measured data were used to prescribe blood flow velocity profiles at the AAo inflow section, at multiple phases of the cardiac cycle (Morbiducci et al. 2013), as explained in the following section. The flow rate waveform in the ascending aorta, as extracted from measured phase data, is presented in Figure 1. It was already observed that the measured velocity profiles at the AAo inflow section are characterized by fully 3D velocity profiles, since the mean value of the measured in-plane velocity component over the inlet section is about 30% of the mean value of the through-plane velocity component, when considering the whole duration of the cardiac cycle (Morbiducci et al. 2013).

2.2. Fluid dynamic model

Blood was assumed a homogeneous, incompressible Newtonian fluid. The finite volume method was applied to solve the fluid motion equations in steady-state conditions:

$$\rho(\mathbf{V} \cdot \nabla)\mathbf{V} + \nabla p - \mu\nabla^2\mathbf{V} = 0 \qquad \nabla \cdot \mathbf{V} = 0 \tag{1}$$

where $\boldsymbol{V}$ is the velocity vector, p is the pressure, ρ is the density (ρ = 1060 kg/m^3) and μ is the dynamic viscosity (μ = 0.0035 Pa·s). The general purpose CFD code Fluent (ANSYS Inc., USA) was used on a computational mesh-grid made of two unstructured meshes created with prismatic and tetrahedral volume elements. Higher cell density was generated near the vessel wall to resolve local velocity gradients.

Steady flow analysis was adopted here to limit the overall computational cost of the Monte Carlo procedure. Three different flow regimes, corresponding to three different phases of the cardiac cycle (Figure 1) were considered: flow regime corresponding to the beginning of the systole (T1), peak systole (T2) and halfway of the systolic deceleration phase (T3). The three flow regimes are characterized by a Reynolds number, at the AAo inlet section, equal to 608, 5138 and 2497, respectively. For each cardiac phase, 3D continuity and Navier–Stokes equations (Equation 1) were solved without turbulence closure, using second-order accuracy and double numerical precision. The simulations were performed on a 5 million mesh for flow regimes T1 and T3 and on a finer 18 million mesh for T2. In both cases, a mesh convergence study was performed to ensure a grid independent solution.

Arterial walls were assumed to be rigid, with no-slip condition on them. Straight flow extensions were added to the four outlet sections (DAo, BCA, LCCA and LSA) to reduce the effect of outflow BCs on the solution. At the end of the flow extensions a stress-free Neumann boundary condition was imposed.

PC-MRI velocity measurements were used to obtain the inlet boundary conditions in terms of velocity profiles at the AAo as detailed elsewhere (Morbiducci et al. 2013, 2015). For each simulated cardiac phase, two different BCs were generated at the AAo inflow section: a 1D (axial) velocity profile, neglecting in-plane velocity components and a fully 3D profile, retaining all the three components of the measured velocity field.

2.3. Stochastic model

The Monte Carlo method was used to propagate the uncertainty in measured PC-MRI velocity profiles applied as inflow BCs, through the CFD model of the aorta. This technique requires random generation of a large ensemble of inputs from their probability distributions and successive deterministic model simulations to generate many realizations of the outputs. In this work, at each cell centroid j (j = 1, 2, … N, being N the number of cells on the

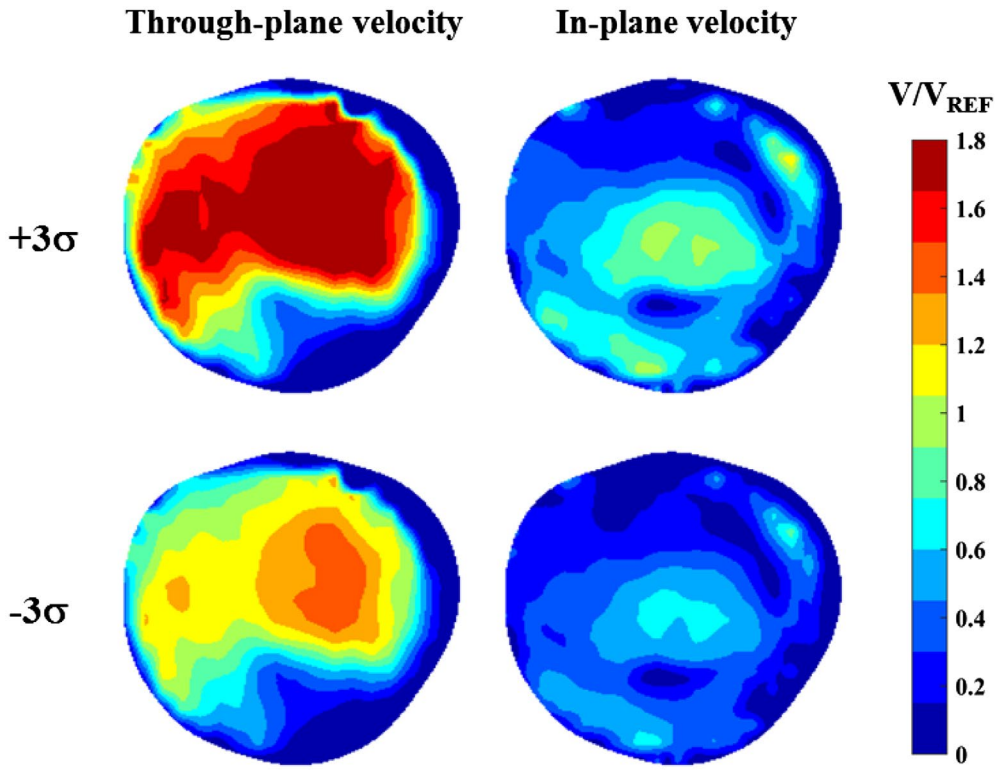

Figure 2. Contour maps of through-plane and in-plane velocity components at the AAo inlet section. Peak systole flow regime (T2) is displayed. Maximum positive (+3σ, upper panel) and negative (-3σ, lower panel) deviation of input velocity data from the PC-MRI measured values. Velocities are normalized with respect to the measured average velocity magnitude over the inlet section (V_{REF}). The contour maps represent the upper and lower limits of variation of all the velocity random samples extracted from the input distribution for the Monte Carlo runs.

inflow section) of the AAo inlet section, each PC-MRI velocity component V_{ij} (i = 1, 2, 3) was assumed to be normally distributed:

$$p\left(V_{ij}\right) = \frac{1}{\sqrt{2\pi\sigma_{ij}^2}} \exp\left(-\frac{\left(V_{ij}-\mu_{ij}\right)^2}{2\sigma_{ij}^2}\right) \qquad (2)$$

where mean μ_{ij} is equal to the measured value and σ_{ij} is the standard deviation. The latter was set by assuming a signal to noise ratio ($SNR = \mu_{ij}/\sigma_{ij}$) of the PC-MRI data equal to 16 (Tresoldi et al. 2014), corresponding to a coefficient of variation ($CV = \sigma_{ij}/\mu_{ij}$) equal to 6.25%. Hence, for a given phase measurement μ_{ij} the standard deviation was set equal to $\sigma_{ij} = \mu_{ij}/16$. The latter would imply a maximum deviation of inlet BC velocity data from the mean value of ±18%, when truncating the normal distribution at ±3σ. An explanatory example of contour maps of the measured PC-MRI velocity data ±3σ is presented in Figure 2, where the upper and lower limits of variation of all the velocity random samples extracted from the input distribution for the Monte Carlo runs are displayed.

A major concern in Monte Carlo simulations is that the accuracy of the results depends on the number of random samples extracted from the input distribution. As a consequence, it is necessary to determine the number of replications required to achieve a desired level of accuracy. In this work, the number of Monte Carlo runs was set equal to 100, which was the minimum value ensuring the convergence of the probability density functions of the output variables. Hence, for each simulated flow regime and each inlet BC scenario, 100 CFD experiments were performed for a total of 600 numerical simulations. Using a Server Rack FUJITSU PRIMERGY RX300S7 equipped with an Intel Xeon E5-2665 processor with 16 computational cores (clock frequency of 2.40 GHz, shared RAM of 96 GB), the wall-clock time of each set of 100 numerical simulations was about 8 and 56 h for the 5 and 18 million mesh cardinality, respectively. Overall, the computational cost of the numerical experiments was about 2400 core hours.

The results of the Monte Carlo simulations were used to estimate the empirical probability density functions of hemodynamic quantities of interest at relevant anatomical landmarks. Namely, the uncertainty in the prediction of vessel cross-section averaged flow quantities was estimated at seven planes perpendicular to local vessel's axis

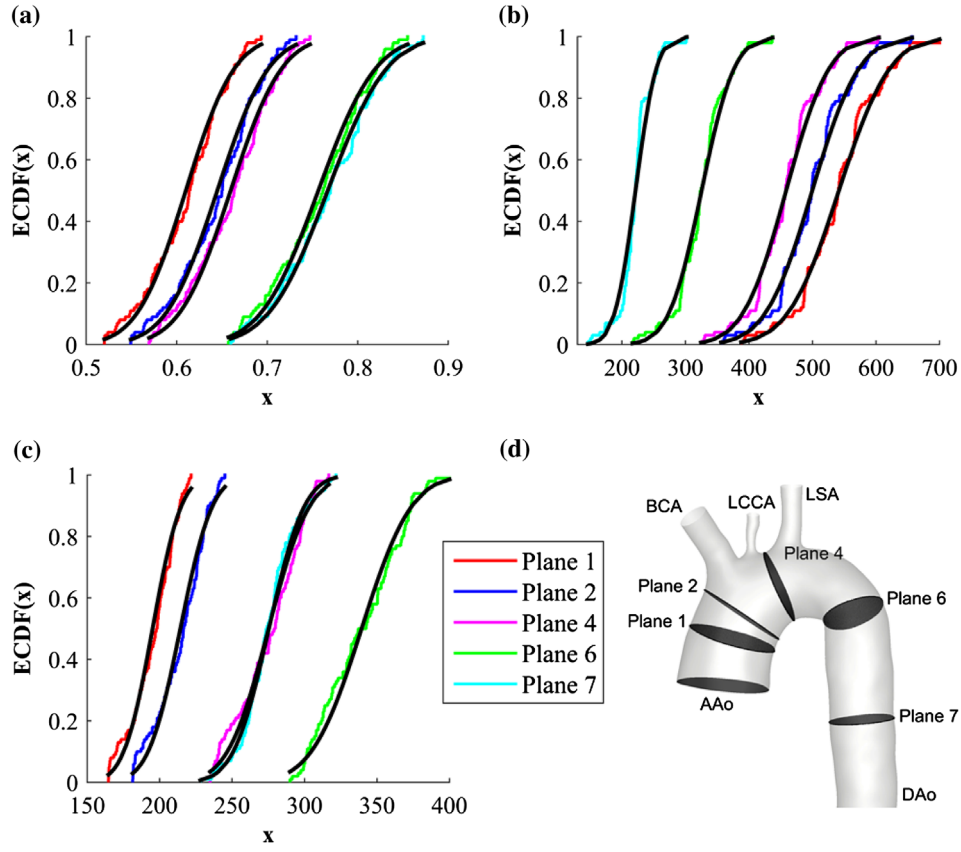

Figure 3. Empirical cumulative distribution functions of cross-section averaged blood velocity magnitude [m/s] (a), pressure [Pa] (b) and vorticity magnitude [1/s] (c) at different positions along the aorta (d), for time instant T2 and 3D velocity inlet profile.

(Figure 1), from plane 1 (located just downstream of the AAo section) to plane 7 (in the descending aorta). An example of the resulting empirical cumulative distribution functions (ECDFs) is reported in Figure 3, for five off the seven planes and for velocity magnitude (a), pressure (b) and vorticity magnitude (c).

Finally, for each plane, mean and standard deviation of the ECDFs of the predicted flow quantities were estimated in order to obtain the signal to noise ratio, which is a measure of the prediction uncertainty.

3. Results and discussion

Figure 4 shows the SNR as estimated from the ECDFs of velocity magnitude (a), pressure (b), and vorticity magnitude (c), for the three flow regimes here investigated. The results were obtained prescribing a fully 3D velocity profile at the inlet section of the AAo, but the same findings were obtained for the 1D velocity profile-based inlet BC strategy.

It can be noticed that the uncertainty affecting the flow quantities is poorly dependent on the location. This means that no specific locations are more affected by the inlet BC uncertainty than others. The results also show that the magnitude of the output uncertainty depends on the flow variable of interest. Uncertainty in pressure is the highest followed by velocity and vorticity magnitude. This is generally true for all the flow regimes investigated.

Table 1 reports the signal to noise ratio, averaged over the seven analysis planes, of the bulk flow variables, for the three phases of the cardiac cycle T1, T2 and T3 and, for each phase, for the two inlet BC strategies (1D and 3D).

It can be noticed that in the 3D case, for flow regimes T1, T2 and T3 the SNR was respectively equal to 14, 15 and 14 for velocity magnitude; 9, 9 and 11 for pressure and 15, 13 and 16 for vorticity magnitude. These data indicate that the predicted uncertainty is always higher than the prescribed input uncertainty (SNR = 16), with the exception of one single case (vorticity magnitude for phase T3). It is noteworthy to observe that the SNR of blood pressure can be up to 40% lower than the one of the uncertainty source. Regarding uncertainty variability with respect to the cardiac phase, no common trends can be identified for the three flow variables. The SNR of velocity magnitude is almost constant for the three cardiac phases, while the SNR of vorticity magnitude exhibits the highest intra-phase variability, with T2 (flow regime corresponding to peak systole) being the most affected by uncertainty.

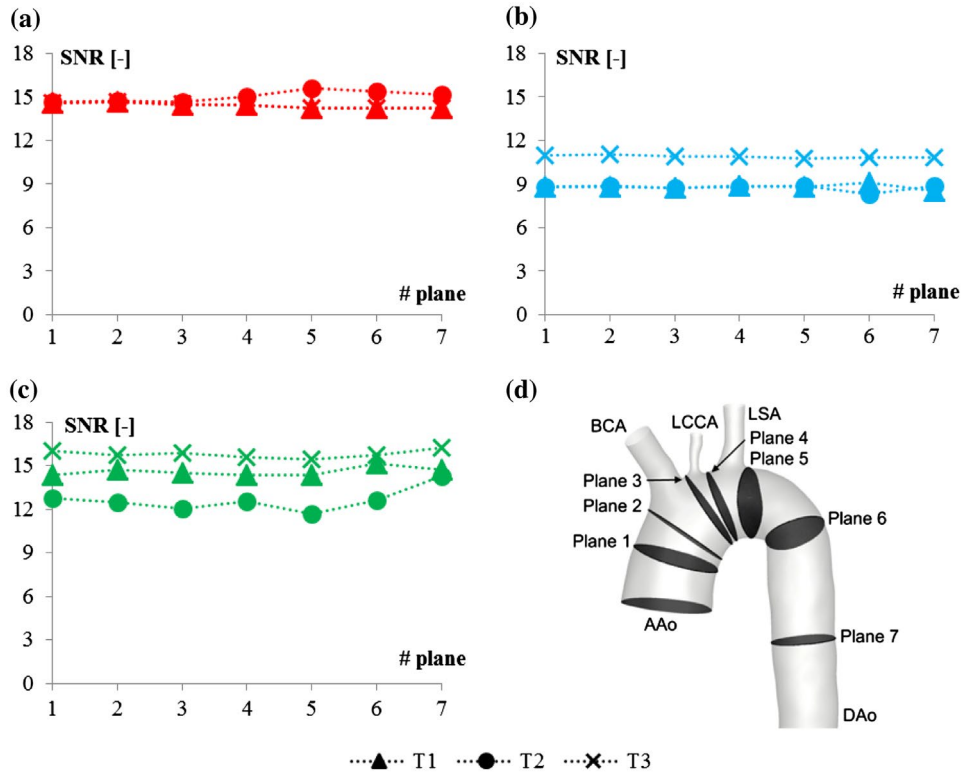

Figure 4. Signal to noise ratio (SNR) of cross-section averaged blood velocity magnitude (a), pressure (b) and vorticity magnitude (c) at different positions along the aorta (d), for three phases of the cardiac cycle. Results are obtained with the 3D velocity inlet profile.

Table 1. Signal to noise ratio (SNR), averaged over the seven analysis planes, of the bulk flow variables, for the three phases of the cardiac cycle T1, T2 and T3 and, for each phase, for the two inlet BC strategies (1D and 3D).

Cardiac phase	BC strategy	Mean SNR velocity magnitude	Mean SNR pressure	Mean SNR vorticity magnitude
T1	1D	14.5	11.1	14.3
T1	3D	14.4	8.8	14.6
T2	1D	14.8	8.8	13.0
T2	3D	15.0	8.7	12.6
T3	1D	14.4	10.9	15.4
T3	3D	14.4	10.9	15.8

Finally, pressure uncertainty is higher in flow regimes T1 and T2, characterized by the same SNR, than in T3.

An additional analysis was performed to investigate the effect of the uncertainty in inlet BCs on wall shear stress (WSS) distribution. Figure 5 shows mean and coefficient of variation of the ECDFs of the WSS distribution at the aortic luminal surface. The results are presented for each investigated flow regime and for the two inlet BC strategies applied here.

It can be noticed that the uncertainty affecting WSS predictions strongly differs between the flow regime corresponding to peak systole and flow regimes T1 and T3. The value of the coefficient of variation averaged over the whole luminal surface is about 10% at flow regimes T1 and T3, and about 30% at T2. Marked differences can also be observed in the spatial distribution of WSS uncertainty. In detail, regions at the luminal surface affected by the highest WSS uncertainty characterize the flow regime T2, with focal maxima at the descending aorta, particularly when using a 1D inlet velocity profile, while at T1 and T3 uncertainty is fairly uniform over all the luminal surface of the vessel. In all the cases investigated here, the uncertainty propagation in WSS calculation resulted to be higher than the input uncertainty (CV = 6.25%).

Regarding the role of the inlet BC strategy, it is somewhat relevant only for flow regime corresponding to peak systole. In this case, both the mean and the CV of the WSS are affected by the inflow condition imposed at the AAo inlet section. It can be observed, by visual inspection, that imposing a 1D velocity profile leads to higher spatial variability of the WSS first and second order statistics.

4. Conclusions

The work presented an uncertainty propagation study aimed at investigating the impact that uncertainty in PC-MRI measurements of velocity profiles has on patient-specific CFD modelling of aortic hemodynamics, when they are prescribed as Dirichlet BCs at the inflow section in the AAo. The uncertainty of blood velocity,

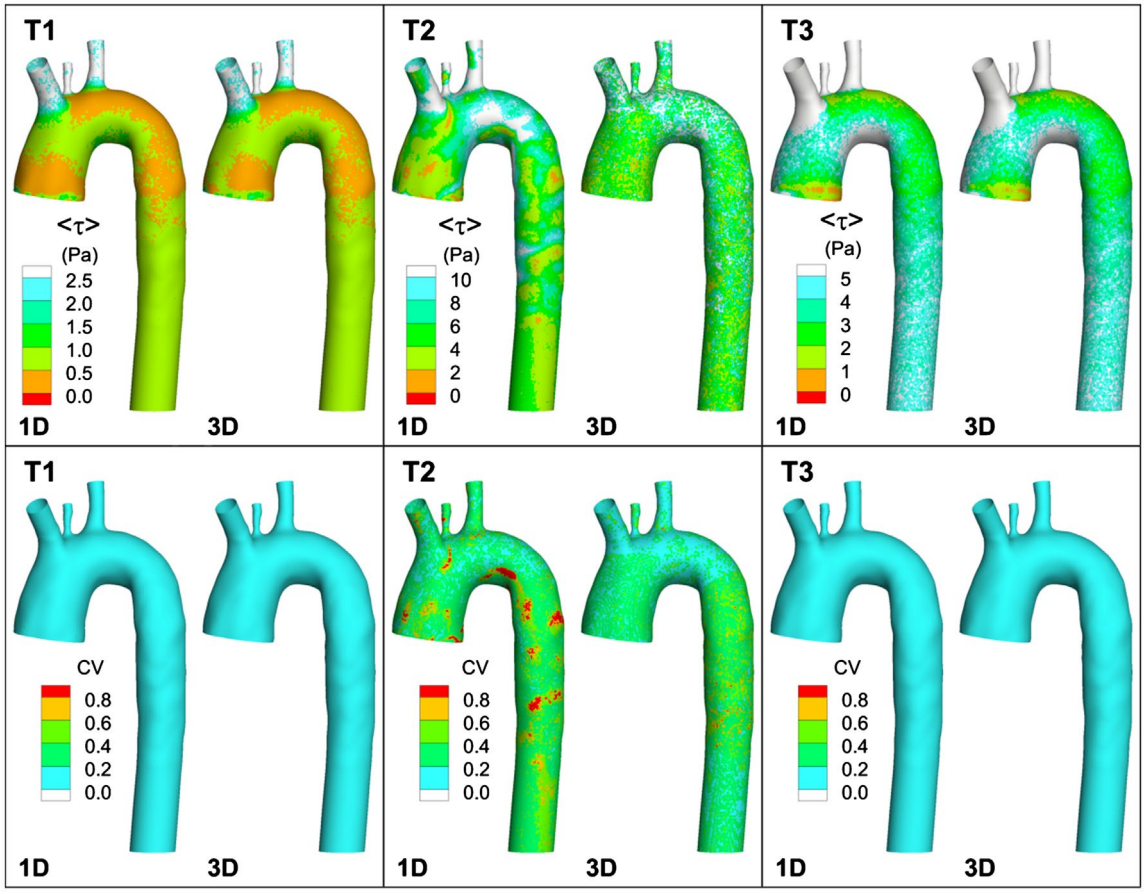

Figure 5. Mean (upper panel) and coefficient of variation (lower panel) of wall shear stress on inner surface of thoracic aorta, at phases T1, T2 and T3 of the cardiac cycle, for 1D and 3D inlet BCs.

pressure and vorticity along the aorta, and of wall shear stress distribution at its luminal surface, was quantified by Monte Carlo simulations with a steady-state Navier–Stokes solver, for three distinct flow regimes, corresponding to three different phases of the cardiac cycle, and for two different inlet BC strategies, i.e. 1D velocity profile (neglecting the measured in-plane velocity and considering only the through-plane velocity component) and fully 3D velocity profile. The main findings of the study are the following:

(1) Propagating the inflow BC uncertainty through the Navier–Stokes equations leads to a decrease in the SNR of CFD predictions with respect to the SNR of the uncertainty source. This result holds for both intravascular flow quantities and WSS distribution, but uncertainty in wall shear stress predictions (particularly at peak systole) is much higher than uncertainty in bulk flow variables. Among the flow variables, blood pressure has the highest predictive uncertainty, followed by velocity and vorticity magnitude: the SNR of blood pressure can be up to 40% lower than the one of the uncertainty source.

(2) Uncertainty affecting intravascular flow quantities does not depend neither on the anatomical location nor on the flow regime. Differently, WSS uncertainty at peak systole is much higher than WSS uncertainty at decelerating/accelerating phases of the systole. Moreover, regions at the luminal surface where high WSS uncertainty (and low WSS mean values) is localized are evident at peak systole, while at the other flow regimes the predictive uncertainty is almost constant over the luminal surface of the vessel.

(3) The effect of the inflow BC strategy (i.e. 1D or 3D velocity profile) on the resulting probability density functions is far from being negligible only for WSS at flow regime corresponding to peak systole.

One major limit of this work is the steady flow assumption. However, it should be noticed that: (1) in the Navier–Stokes equations, uncertainty is mainly propagated by the acceleration operator $\left(\frac{\partial \mathbf{V}}{\partial t} + (\mathbf{V} \cdot \nabla)\mathbf{V}\right)$, where the non-linear advective contribution $(\mathbf{V} \cdot \nabla)\mathbf{V}$, is expected to be predominant, compared to the local linear term $\frac{\partial \mathbf{V}}{\partial t}$; (2)

the computational cost of an unsteady simulation is about 2 orders of magnitude higher that one of a steady simulation, hence Monte Carlo unsteady experiments are not affordable unless resorting to high performance computing platforms; (3) some authors claim that the resulting time averaged stress tensor does not substantially differ from the unsteady flow solution (e.g. Karmonik et al. 2014; Caballero & Laín 2015).

In this study, the same VENC value was adopted for different phase velocity components, and along the entire cardiac cycle. Since the phase contrast image noise is function of the VENC value (see Equation 3), the applied VENC strategy could influence uncertainty propagation in computational hemodynamics, in particular at time points along the cardiac cycle when blood velocity is low (i.e. during late diastole). Although higher *SNR* levels could potentially be obtained by, e.g. setting different VENC values for the three phase velocity components, the applicability of the proposed method to study uncertainty propagation is still valid.

The methodology proposed here to estimate uncertainty propagation of PC-MRI derived inlet boundary conditions in computational hemodynamics models is focused on the healthy human thoracic aorta, and does not explore, at this stage, uncertainty propagation in the altered hemodynamics associated with a specific pathology. However, this does not entail the generality of the results because the extension of the approach to study uncertainty propagation in computational hemodynamics models of diseased cardiovascular districts is straightforward. Moreover, the consideration of healthy aorta hemodynamics is of relevant interest for at least three main reasons: (1) healthy aorta hemodynamics represent the essential frame of reference to which altered hemodynamics, associated with pathology, has to be compared with; (2) the study of hemodynamics of healthy aorta adds basic knowledge to the interpretation of the physiological role played by peculiar hemodynamic structures (in relation to, e.g. ageing); (3) healthy arterial segments have been used for several years to study the hemodynamic risk factor associated with the onset of vessel wall pathologies (e.g. atherosclerosis).

For these reasons, the methodological approach proposed here does make scientific sense and paves the way to further investigations, adopting more efficient stochastic methods to propagate input uncertainty into output variables of interest in more realistic, time-dependent simulation scenarios.

The study demonstrates that uncertainty related to PC-MRI phase flow measurements, when adopted as inflow BCs in terms of velocity profiles in computational hemodynamic models of human aorta, propagates not only to intravascular flow, but also to shear stress distribution at vessel wall. The approach here adopted emphasizes that the PC-MRI flow measurements-derived uncertainty is an important source of uncertainty. This is of utmost importance considering that it is non-linearly related with other uncertainties intrinsic in modeling assumptions such as aortic wall distensibility (Lantz et al. 2011; Brown et al. 2012), outflow boundary conditions (Gallo et al. 2012), blood rheological properties (Liu et al. 2011), etc. As a consequence, the global effect cannot be neglected when looking at model reliability.

Disclosure statement

No potential conflict of interest was reported by the authors.

Funding

This work was partially supported by the Italian research program, Ministero dell'Istruzione, dell'Università e della Ricerca [PRIN 2009] 'Development and validation of hybrid models for the implementation of patient specific hemodynamics analysis as a tool to support the clinical practice'.

References

Brown AG, Shi Y, Marzo A, Staicu C, Valverde I, Beerbaum P, et al. 2012. Accuracy vs. computational time: Translating aortic simulations to the clinic. J. Biomech. 45:516–523.

Caballero AD, Laín S. 2015. Numerical simulation of non-Newtonian blood flow dynamics in human thoracic aorta. Comput Methods Biomech Biomed Eng. 18(11):1200–1216.

D'Elia M, Veneziani A. 2013. Uncertainty quantification for data assimilation in a steady incompressible Navier–Stokes problem. ESAIM Math Model Numer Anal. 47(4):1037–1057.

Eck VG, Donders WP, Sturdy J, Feinberg J, Delhaas T, Hellevik LR, Huberts W. 2016. A guide to uncertainty quantification and sensitivity analysis for cardiovascular applications. Int J Numer Method Biomed Eng. 32(8):02755.

Eck VG, Sturdy J, Hellevik LR. 2017. Effects of arterial wall models and measurement uncertainties on cardiovascular model predictions. J Biomech. 50:188–194.

Gallo D, De Santis G, Negri F, Tresoldi D, Ponzini R, Massai D, Deriu MA, Segers P, Verhegghe B, Rizzo G, Morbiducci U. 2012. On the use of *in vivo* measured flow rates as boundary conditions for image-based hemodynamic models of the human aorta: implications for indicators of abnormal flow. Ann Biomed Eng. 40(3):729–741.

Grinberg L, Karniadakis GEM. 2008. Outflow boundary conditions for arterial networks with multiple outlets. Ann Biomed Eng. 36:1496–1514.

Huberts W, Van Canneyt K, Segers P, Eloot S, Tordoir JHM, Verdonck P, van de Vosse FN, Bosboom EMH. 2012. Experimental validation of a pulse wave propagation model for predicting hemodynamics after vascular access surgery. J Biomech. 45(9):1684–1691.

Javadzadegan A, Yong ASC, Chang M, Ng MNC, Behnia M, Kritharides L. 2016. Haemodynamic assessment of human coronary arteries is affected by degree of freedom of artery movement. Comput Methods Biomech Biomed Eng. 260–272. doi:10.1080/10255842.2016.1215439.

Jin S, Oshinski J, Giddens DP. 2003. Effects of wall motion and compliance on flow patterns in the ascending aorta. J Biomech Eng. 125:347–354.

Karmonik C, Partovi S, Schmack B, Weymann A, Loebe M, Noon GP, Piontek P, Karck M, Lumsden AB, Ruhparwar A. 2014. Comparison of hemodynamics in the ascending aorta between pulsatile and continuous flow left ventricular assist devices using computational fluid dynamics based on computed tomography images. Artif Organs. 38(2):142–148.

Lantz J, Renner J, Karlsson M. 2011. Wall shear stress in a subject specific human aorta — influence of fluid-structure interaction. Int. J. Appl. Mech. 3(4):759–778.

Lee SW, Steinman DA. 2007. On the relative importance of rheology for image-based CFD models of the carotid bifurcation. J Biomech Eng. 129(2):273–278.

Liu X, Fan Y, Deng X, Zhan F. 2011. Effect of non-Newtonian and pulsatile blood flow on mass transport in the human aorta. J. Biomech. 44(6):1123–1131.

Morbiducci U, Ponzini R, Rizzo G, Cadioli M, Esposito A, De Cobelli F, Del Maschio A, Montevecchi FM, Redaelli A. 2009. *In vivo* quantification of helical blood flow in human aorta by time-resolved three-dimensional cine phase contrast magnetic resonance imaging. Ann Biomed Eng. 37(3):516–531.

Morbiducci U, Ponzini R, Rizzo G, Cadioli M, Esposito A, Montevecchi FM, Redaelli A. 2011a. Mechanistic insight into the physiological relevance of helical blood flow in the human aorta: an in vivo study. Biomech Model Mechanobiol. 10:339–355.

Morbiducci U, Gallo D, Massai D, Ponzini R, Deriu MA, Antiga L, Redaelli A, Montevecchi FM. 2011b. On the importance of blood rheology for bulk flow in hemodynamic models of the carotid bifurcation. J Biomech. 44:2427–2438.

Morbiducci U, Ponzini R, Gallo D, Bignardi C, Rizzo G. 2013. Inflow boundary conditions for image-based computational hemodynamics: impact of idealized versus measured velocity profiles in the human aorta. J Biomech. 46(1):102–109.

Morbiducci U, Gallo D, Cristofanelli S, Ponzini R, Deriu MA, Rizzo G, Steinman DA. 2015. A rational approach to defining principal axes of multidirectional wall shear stress in realistic vascular geometries, with application to the study of the influence of helical flow on wall shear stress directionality in aorta. J Biomech. 48:899–906.

Quarteroni A, Veneziani A, Vergara C. 2016. Geometric multiscale modeling of the cardiovascular system, between theory and practice. Comput Methods Appl Mech Eng. 302:193–252.

Quicken S, Donders WP, van Disseldorp EMJ, Gashi K, Mees BME, van de Vosse FN, et al. 2016. Application of an adaptive polynomial chaos expansion on computationally expensive three-dimensional cardiovascular models for uncertainty quantification and sensitivity analysis. J Biomech Eng. 138(12):121010.

Sankaran S, Marsden AL. 2011. A stochastic collocation method for uncertainty quantification and propagation in cardiovascular simulations. J Biomech Eng. 133(3):031001.

Sankaran S, Grady L, Taylor C. 2015. Impact of geometric uncertainty on hemodynamic simulations using machine learning. Comput Methods Appl Mech Eng. 297:167–190.

Sankaran S, Kim HJ, Choi G, Taylor CA. 2016. Uncertainty quantification in coronary blood flow simulations: impact of geometry, boundary conditions and blood viscosity. J Biomech. 49(12):2540–2547.

Schiavazzi DE, Arbia G, Baker C, Hlavacek AM, Hsia TY, Marsden AL, Vignon-Clementel IE, The Modeling of Congenital Hearts Alliance (MOCHA) Investigators. 2016. Uncertainty quantification in virtual surgery hemodynamics predictions for single ventricle palliation. Int. J. Numer. Meth. Biomed. Eng. 32(3):e02737. doi:10.1002/cnm.2737.

Spilker RL, Taylor CA. 2010. Tuning Multidomain Hemodynamic Simulations to Match Physiological Measurements. Annals of Biomedical Engineering. 38(8):2635–2648.

Taylor CA, Steinman DA. 2010. Image-based modelling of blood flow and vessel wall dynamics: applications, methods and future directions. Annal Biomed Eng. 38(3):1188–1203.

Tiago J, Gambaruto A, Sequeira A. 2014. Patient-specific blood flow simulations: setting Dirichlet boundary conditions for minimal error with respect to measured data. Math Model Nat Phenom. 9(6):98–116.

Tran JS, Schiavazzi DE, Ramachandra AB, Kahn AM, Marsden AL. 2017. Automated tuning for parameter identification and uncertainty quantification in multi-scale coronary simulations. Computers Fluids. 142:128–138.

Tresoldi D, Cadioli M, Ponzini R, Esposito A, De Cobelli F, Morbiducci U, Rizzo G. 2014. Mapping aortic hemodynamics using 3D cine phase contrast magnetic resonance parallel imaging: evaluation of an anisotropic diffusion filter. Magn Reson Med. 71(4):1621–1631.

Valen-Sendstad K, Piccinelli M, KrishnankuttyRema R, Steinman DA. 2015. Estimation of inlet flow rates for image-based aneurysm CFD models: where and how to begin? Annal Biomed Eng. 43(6):1422–1431.

Veneziani A, Vergara C. 2005. Flow rate defective boundary conditions in hemodynamics simulations. Int J Numer Methods Fluids. 47:803–816.

Volonghi P, Tresoldi D, Cadioli M, Usuelli AM, Ponzini R, Morbiducci U, Esposito A, Rizzo G. 2016. Automatic extraction of three-dimensional thoracic aorta geometric model from phase contrast MRI for morphometric and hemodynamic characterization. Magn Res Med. 75(2):873–882.

Zhao SZ, Xu XY, Hughes AD, Thom SA, Stanton AV, Ariff B, Long Q. 2000. Blood flow and vessel mechanics in a physiologically realistic model of a human carotid arterial bifurcation. J Biomech. 33(8):975–984.